Decadal Variability of Great Lakes Ice Cover in Response to AMO and PDO, 1963–2017

JIA WANG,[a] JAMES KESSLER,[b] XUEZHI BAI,[c] ANNE CLITES,[a] BRENT LOFGREN,[a] ALEXANDRE ASSUNCAO,[b] JOHN BRATTON,[d] PHILIP CHU,[a] AND GEORGE LESHKEVICH[a]

[a] *NOAA/Great Lakes Environmental Research Laboratory, Ann Arbor, Michigan*
[b] *Cooperative Institute for Great Lakes Research, University of Michigan, Ann Arbor, Michigan*
[c] *Hohai University, Nanjing, China*
[d] *LimnoTech, Ann Arbor, Michigan*

(Manuscript received 27 April 2017, in final form 26 April 2018)

ABSTRACT

In this study, decadal variability of ice cover in the Great Lakes is investigated using historical airborne and satellite measurements from 1963 to 2017. It was found that Great Lakes ice cover has 1) a linear relationship with the Atlantic multidecadal oscillation (AMO), similar to the relationship of lake ice cover with the North Atlantic Oscillation (NAO), but with stronger impact than NAO; 2) a quadratic relationship with the Pacific decadal oscillation (PDO), which is similar to the relationship of lake ice cover to Niño-3.4, but with opposite curvature; and 3) decadal variability with a positive (warming) trend in AMO contributes to the decreasing trend in lake ice cover. Composite analyses show that during the positive (negative) phase of AMO, the Great Lakes experience a warm (cold) anomaly in surface air temperature (SAT) and lake surface temperature (LST), leading to less (more) ice cover. During the positive (negative) phase of PDO, the Great Lakes experience a cold (warm) anomaly in SAT and LST, leading to more (less) ice cover. Based on these statistical relationships, the original multiple variable regression model established using the indices of NAO and Niño-3.4 only was improved by adding both AMO and PDO, as well as their interference (interacting or competing) mechanism. With the AMO and PDO added, the correlation between the model and observation increases to 0.69, compared to 0.48 using NAO and Niño-3.4 only. When November lake surface temperature was further added to the regression model, the prediction skill of the coming winter ice cover increased even more.

1. Introduction

The Laurentian Great Lakes are located in the midlatitude area of eastern North America (Fig. 1). The westerly jet stream is located aloft at varying latitudes in the region. The fluctuation of the westerly jet stream is controlled by the North America ridge–trough system (Bai and Wang 2012), which is influenced by large-scale atmospheric teleconnection patterns such as El Niño–Southern Oscillation (ENSO) and the North Atlantic Oscillation (NAO) (Wang et al. 2010; Bai et al. 2012), as well as the Atlantic multidecadal oscillation (AMO) and Pacific decadal oscillation (PDO). The fluctuation of the jet stream causes large variations in the Great Lakes region on synoptic, seasonal, and interannual time scales, leading to large uncertainty in the prediction of regional climate and ice cover.

The teleconnection patterns in both the Pacific and the Atlantic should have impacts on the Great Lakes regional climate and ice cover through influencing the ridge–trough system over North America, which determines the pathway and strength of the westerly jet stream (Bai and Wang 2012). The Pacific ENSO and PDO are located upstream of the Great Lakes, while the NAO and AMO are located downstream along the westerly jet. Any anomalies of upstream and downstream caused by these four patterns would change the ridge–trough intensity and pathway of the jet stream over North America. Therefore, the combined effects of these teleconnection patterns can significantly change lake ice cover through the advection of surface air temperature (SAT) by the jet stream. This is the key underlying dynamic process, even though a single pattern

Denotes content that is immediately available upon publication as open access.

Corresponding author: Jia Wang, jia.wang@noaa.gov

DOI: 10.1175/JCLI-D-17-0283.1

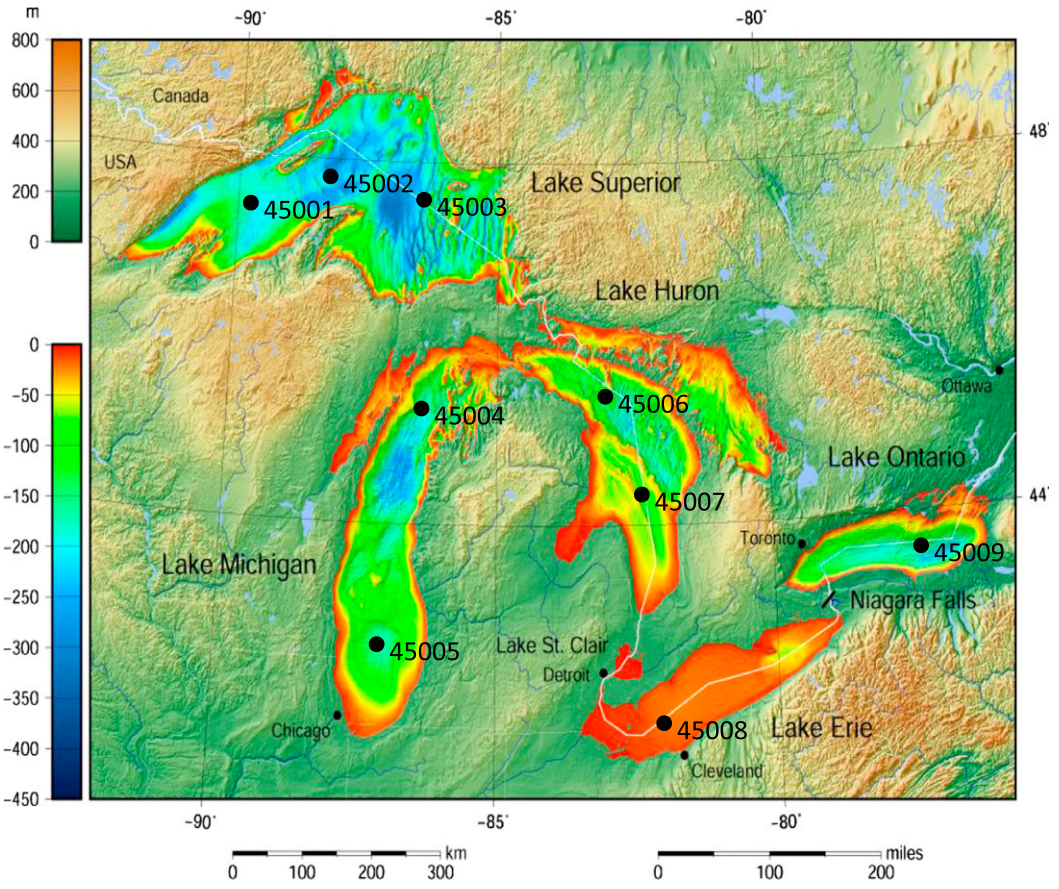

FIG. 1. The Great Lakes region, topography, and bathymetry. For Lakes Superior, Michigan, Huron, St. Clair, Erie, and Ontario, the average water depths are 148, 84, 59, 3, 19, and 85 m, respectively, and the average surface areas are 82 400, 58 000, 59 596, 1114, 25 744, and 19 500 km^2, respectively. Locations of the nine NDBC buoys are labeled.

may not be statistically significantly correlated with lake ice (Mishra et al. 2011; Bai et al. 2012).

Bai et al. (2012) conducted a systematic review of literature on Great Lakes climate and ice cover. Through thorough data synthesis, they revealed several important findings: 1) Great Lakes ice cover and NAO have a linear relationship, 2) Great Lakes ice cover and Niño-3.4 have a quadratic relationship, which is consistent with the nonlinear relationship between ENSO and the SAT (Wu et al. 2005), and 3) both Niño-3.4 and NAO have competing impacts on lake ice cover; however, neither of them dominate. Based on these findings, a regression model was established to hindcast the lake ice cover, using NAO and Niño-3.4 indices only, yielding simulated results that correspond to observed ice cover with a correlation of 0.50 for the period 1963–2011. This regression model was used to project lake ice cover since 2010; however, some extreme (both mild and severe) ice covers were muted, that is, ice in severe winters was underestimated and ice in mild winters was overestimated. Although this model has been used since early winter of 2010 (between late December and early January) to project annual maximum ice coverage (AMIC) each year using the projected NAO and Niño-3.4 indices, it was often seen that the predicted AMIC was systematically lower than the observed AMIC in the severe winters. This indicates that some important predictive factors were missing. For example, this model was used to project AMIC to be 63% in the 2013/14 season, while the measured AMIC was 93% on 24 February 2014. The relative error of 30% was too large to be satisfactory in practice. Therefore, one important, practical motivation is to use the validated regression models developed here to project Great Lakes seasonal AMIC using projected indices of the teleconnection patterns.

The idea to project lake ice cover directly using the indices of teleconnection patterns is based on the previous diagnostic studies. Generally speaking, teleconnection patterns control the sea level pressure (SLP) pattern (i.e., the wind pattern, which causes warm or

cold anomalous SAT by dynamical advection). Winter SAT has an inverse correlation with lake ice cover with a coefficient of about −0.8 (Bai et al. 2011, 2012). At the same time, teleconnection patterns also influence water temperature and water heat content, which in turn affects ice formation. The teleconnection–SLP–SAT cause–effect mechanism only takes into account the SAT effect, but not other factors. However, it should be noted that the observed lake ice cover includes all environmental effects, not only from the teleconnection–SLP–SAT mechanism, but also from water temperature and its (depth dependent) heat content (Fig. 1), as well as other factors such as runoff, air–ice–lake energy transport, and advection of heat into and out of the region. Therefore, using teleconnection indices to forecast lake ice cover should add more to the model than using SLP (i.e., wind field) and SAT only on the seasonal time scales, because seasonal projection of local SAT is not as reliable as the global teleconnection indices.

Wang et al. (2012a) examined both temporal and spatial variability of Great Lakes ice cover for the period 1973–2010. The first mode of lake ice is associated with the NAO, which significantly influences SAT on the Great Lakes, while the second mode of lake ice is associated with the ENSO-like Pacific pattern, which has a nonlinear impact on SAT on the Great Lakes because the zero line of the anomaly is across the midbasin of the Great Lakes dividing the north (positive SAT anomaly) and the south (negative SAT anomaly). A large negative trend in annual average ice cover was observed. With the last seven years of data added to the ice dataset (Wang et al. 2012b, 2017a), particularly with high ice cover during the 2013/14 and 2014/15 winters, an update of the data is necessary for better understanding of the mechanisms of decadal and multidecadal variability in lake ice.

Previous studies (Magnuson et al. 2000; Ghanbari et al. 2009; Weyhenmeyer et al. 2011; Mishra et al. 2011) showed that there is a weak linear relationship between little lake ice cover in North America and the AMO and PDO, in addition to, ENSO and NAO, or the Arctic Oscillation (AO). No further investigations combining these patterns were conducted. In other words, no quantitative relationships were derived, although they qualitatively revealed the relationships to some degree.

The purpose of this study is to 1) investigate decadal variability of Great Lakes ice cover and associated atmospheric dynamic processes, 2) reveal the underlying mechanisms of the lake ice decadal variability in response to AMO and PDO, and 3) establish updated regression models for better hindcasting of seasonal lake ice cover using the indices of teleconnection patterns, which can be used to project seasonal lake ice cover using projected indices of these teleconnection patterns.

2. The data

a. Great Lakes ice dataset

AMIC for the Great Lakes is defined as the greatest percentage of lake surface area covered by ice each winter. AMIC for each lake and the Great Lakes as a whole for winters 1963–2017 was calculated using the dataset archived at the NOAA/Great Lakes Environmental Research Laboratory (Assel et al. 2003; Wang et al. 2012b, 2017a,b; https://www.glerl.noaa.gov/data/ice/#historical), which is largely based on ice charts produced by the U.S. National Ice Center. Systematic lake-scale observations of Great Lakes ice cover began in the 1960s by federal agencies in the United States (U.S. Army Corps of Engineers and U.S. Coast Guard) and Canada (Atmospheric Environment Service and Canadian Coast Guard) to support early- and late-season navigation, the closing of the navigation season in winter, and the opening of navigation in spring. Observations were made at irregular intervals primarily to support operational activities. Ice charts depicting ice concentration patterns and ice extent during 1963–72 were constructed from side-looking airborne radar imagery and visual aerial ice reconnaissance (Assel and Rodionov 1998).

Systematic satellite measurements have been available since 1973. Two datasets were used in this study; one is from the Canadian Ice Service (CIS) and the other is from the U.S. National Ice Center (NIC), a cooperative effort between the U.S. Navy, NOAA, and the Coast Guard. The CIS data span the time period from 1973 to 1988. From 1989 to present, these agencies have coordinated their data. During the ice year, each agency has at least one chart per week—more frequently during ice onset and ice offset periods to aid navigation. Starting in 2011, the charts have been produced daily. The 1973 ''ice year'' refers to the period from November 1972 to May 1973. Ice concentration was derived from NIC Great Lakes ice analysis charts, which are based on satellite products from RadarSat, *Environmental Satellite* (*Envisat*), Advanced Very High Resolution Radiometer (AVHRR), Geostationary Operational Environmental Satellite (GOES), Moderate Resolution Imaging Spectroradiometer (MODIS), and other available data.

The normalized AMIC is defined as the difference between the AMIC and its climatology (mean), divided by its standard deviation. The AMIC of the whole Great Lakes has a significant negative correlation (∼−0.8) with the Great Lakes area-averaged winter SAT during

the period 1963–2010, indicating that the interannual variability of Great Lakes ice cover is mainly controlled by the SAT (Bai et al. 2011). Although Great Lakes ice cover is closely correlated with the overlying SAT, there is some complexity in the causal relationship, as the lake and air can act as sources and sinks of heat for each other. Advection of heat from other regions plays a large role in the availability of heat for the lake–atmosphere system in the immediate Great Lakes region.

b. Climate indices

The Niño-3.4 sea surface temperature (SST) anomaly index was used as a marker of ENSO variability to identify the warm and cold episodes during 1963–2017 based on a threshold of ±0.5°C. Cold and warm episodes are defined as those periods for which the threshold is met for a minimum of five consecutive overlapping seasons such as November–January (NDJ), December–February (DJF), January–March (JFM), and so on. Otherwise, the winter is defined as ENSO neutral. The index is defined as the 3-month running mean of Extended Reconstructed Sea Surface Temperature, version 3 (ERSST.v3), SST anomalies in the Niño-3.4 region [5°N–5°S, 120°–170°W; obtained from the NOAA/Climate Prediction Center (CPC) online at http://www.cpc.noaa.gov/products/analysis_monitoring/ensostuff/ensoyears.shtml]. The strong warm (cold) winters are defined as the DJF periods when the mean index exceeds 1.0°C (−1.0°C), and weak warm and cold winters are defined as DJF periods when the mean index has anomalies between 0.5° and 1.0°C.

The monthly NAO index from 1963 to 2017 was obtained from the University of East Anglia Climatic Research Unit, United Kingdom (available online at http://crudata.uea.ac.uk/cru/data/nao/). The NAO is defined as the normalized sea level pressure difference between the Azores and Iceland. A winter is defined as having a positive (negative) phase when the DJF mean index exceeds +0.5 (−0.5) standard deviation; otherwise a winter is defined as NAO neutral.

The PDO index is the leading empirical orthogonal function (EOF) of monthly sea surface temperature anomalies (SSTAs) over the North Pacific (poleward of 20°N) after the global mean SST has been removed. The PDO index is the standardized principal component time series (Mantua et al. 1997; Zhang et al. 1997) (available online at http://research.jisao.washington.edu/pdo/PDO.latest and https://www.ncdc.noaa.gov/teleconnections/pdo/).

The AMO was identified by Schlesinger and Ramankutty (1994). The AMO signal is usually defined from the patterns of SST variability in the North Atlantic once any linear trend has been removed. This detrending is intended to remove the influence of greenhouse gas–induced global warming from the analysis (Ting et al. 2009). The AMO index was obtained online from http://www.esrl.noaa.gov/psd/data/timeseries/AMO/.

c. Lake surface temperature

Satellite-measured lake surface temperature (LST) over the Great Lakes for the period 1995–2016 was obtained from the Great Lakes Surface Environmental Analysis (GLSEA; available online at https://coastwatch.glerl.noaa.gov/glsea/glsea.html). The monthly values were used to produce the seasonal climatology; then the monthly or winter (January, February, and March) and summer (July, August, and September) anomaly maps were derived by subtracting the climatology.

Buoy LST data, available from 1982 to 2016, for the Great Lakes were from the National Data Buoy Center (NDBC). There are three buoys (45001, 45002, and 45003) in Lake Superior, two (45004 and 45005) in Lake Michigan, two (45006 and 45007) in Lake Huron, and one (45008) in Lake Erie (see Fig. 1 for location). Buoy data for Lake Ontario start in 2002, and thus were not included. These time series were used to construct a regression model.

d. Methods

The methods used in this study include scattering analysis, correlation analysis, composite analysis, and multivariable regression. Following the scatter analysis of the relationships between the AMIC and the NAO and ENSO (Bai et al. 2012), the relationships between the AMIC and the AMO and PDO are established. Using correlation analysis, the correlation coefficients between the AMIC and the AMO and PDO are quantitatively identified. Based on the linear or nonlinear relationship between the AMIC and the AMO and PDO, multivariable regression models using R software are constructed, including their interference or interaction (i.e., competing) mechanism between each two teleconnection patterns.

Composite analysis is a conventional method to show the representations associated with a certain climate event such as the AMO and PDO in this study by averaging the data over the warm and cold years (phases). Because of the small samples available in this study, the Student's t distribution was used to determine the statistical significance between the means of the two samples. Comparing the differences between the two means using the Student's t test requires two independent samples of sizes n_1 and n_2, which possess means and standard deviations given by $\overline{x}_1$ and $\overline{x}_2$ and s_1 and s_2, respectively. Our null hypothesis H_0 is when the two samples are statistically indistinguishable from each other. To test H_0, we use the conventional t score

$$t = \frac{\bar{x}_1 - \bar{x}_2}{\sqrt{\dfrac{(n_1 - 1)s_1^2 + (n_2 - 1)s_2^2}{n_1 + n_2 - 2}\left(\dfrac{1}{n_1} + \dfrac{1}{n_2}\right)}}, \quad (1)$$

which is a value of a random variable having a t distribution with $n_1 + n_2 - 2$ degrees of freedom. The null hypothesis is rejected if the two-tailed t score exceeds the 95% confidence interval.

To measure the regression model's skill for reproducing the measurements, a statistical measure is introduced to conduct the model–data comparison. Root-mean-square deviation (RMSD) is defined as

$$\mathrm{RMSD} = \left[\frac{\sum_{i=1}^{N}(x_i - y_i)^2}{N}\right]^{1/2}, \quad (2)$$

where x_i and y_i ($i = 1, 2, 3, \ldots, N$) are the modeled and observed time series of any variable such as ice area, LST, and so on, and N is the total sampling number. RMSD measures the absolute error of the modeled time series against observation.

To measure the statistical importance of a correlation between two time series, the significance level in this study is estimated by a Monte Carlo simulation (Livezey and Chen 1983; Wang et al. 1994). This method includes four basic steps: 1) randomize one of the original time series; 2) retrieve the original lag-1 autocorrelation in all random series; 3) calculate the correlation coefficients between the original time series and the randomized time series; and 4) find the critical value at which only 5% of coefficients obtained in step 3 are above this value (i.e., the significance level).

3. Results

a. Monthly mean AMIC over 1973–2017

Figure 2 shows the spatial distribution of Great Lakes monthly AMIC for December–April averaged over the period 1973–2017. In late November–early December, ice starts to form along the shallow coasts and embayments in Lake Superior and progresses into January from north to south, reaching the maximum ice cover in February in the southern lakes (Lakes Erie and Ontario) and in March in the northern lakes (Lakes Superior and Huron). Ice gradually decays in April.

b. Decadal variability

The decadal variability in small lakes was investigated by previous studies (Magnuson et al. 2000; Ghanbari et al. 2009; Weyhenmeyer et al. 2011). However, no further quantitative modeling was conducted. Here, by extending the previous time series (1973–2010; Wang et al. 2012a) with the last 7 years (2011–17) as well as the preceding 10 years (1963–72), decadal variability further stands out (Figs. 3 and 4). During this 54-yr period, four high ice bands stand out: 1963–64, 1977–79, 1994, and 2014–15 (Clites et al. 2014), with separation periods of 15, 17, and 21 years, respectively. Figure 4 shows the spatial maps of the record-breaking years of 1979, 1994, and 2014. Similarly, four low ice bands also stand out: 1964–65, 1983, 1998–2002, and 2010–2013, separated by around 20, 18, and 12 years, respectively. The longest low ice band started in 1998 and lasted to 2013. The 1997/98 El Niño was the largest El Niño event in the twentieth century, which may be associated with a regime shift in lake ice cover (Van Cleave et al. 2014) and other environmental components. Note that the 2015/16 El Niño event was the strongest event of the twenty-first century, which was stronger than the 1997/98 event. This is part of the remarkable downward trend observed (Fig. 3; Wang et al. 2012a), which can be attributed to a combination of multidecadal variability and human-caused secular climate warming. The 5-yr running mean indicates that the decadal variability in lake ice has a largest peak in 1981 and a smallest peak in 2002, with a downward trend superimposed with large interannual variability.

4. Great Lakes ice cover in response to AMO and PDO

a. PDO and AMO teleconnection patterns and their impact on the Great Lakes

The PDO is similar to ENSO in spatial impact on Northern Hemisphere climate, but on decadal time scales. As its name would suggest, the PDO lasts decades—usually between 10 and 30 years. The impact of the PDO is primarily a contrast between the eastern tropical Pacific and the North Pacific, and North America (similar to ENSO). During its warm phase, the east Pacific tropics have a warm SST anomaly, and the North Pacific has a cold anomaly, and vice versa during its cold phase. As a result, there is a warm anomaly in northwestern North America and a cold anomaly in southeastern North America. The Great Lakes are located between the high and low centers of SAT or on the edges of both. In other words, any changes in location of these two action centers would swing the Great Lakes from one center to the other, adding complexity to the analysis.

The AMO addresses variability in SST in the North Atlantic Ocean. It has a quasi-cycle of around either

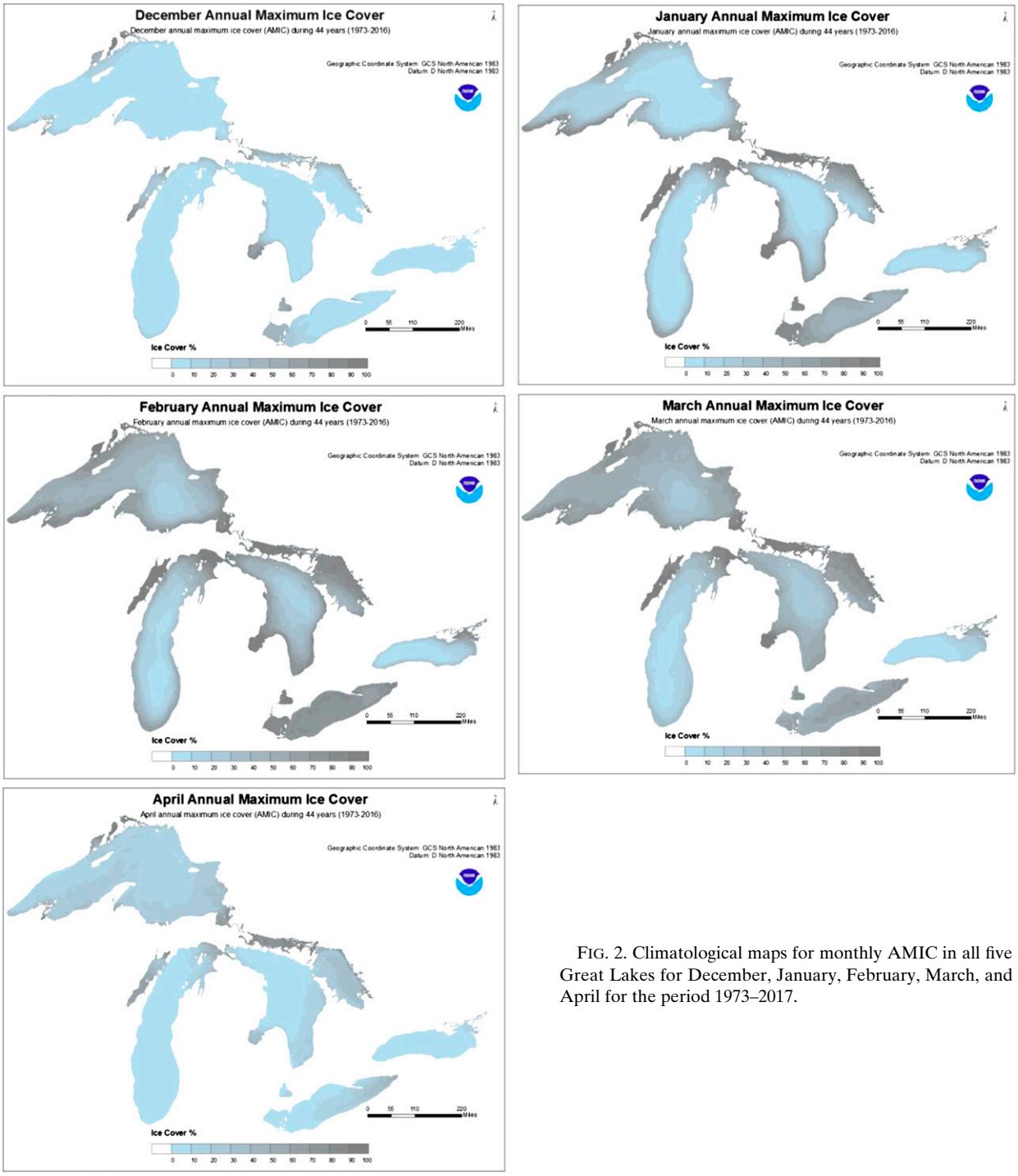

FIG. 2. Climatological maps for monthly AMIC in all five Great Lakes for December, January, February, March, and April for the period 1973–2017.

70 or 50–90 years (Ting et al. 2009). The AMO is associated with the thermohaline circulation in the North Atlantic Ocean. There are two phases in the AMO: warm and cold. The warm phase strengthens North Atlantic tropical cyclone activity because warmer SST provides more moisture to the tropical storms and hurricanes (Zhang and Delworth 2006). Recent research suggested that the AMO is related to the past occurrence of major droughts in the U.S. Midwest and the Southwest. When the AMO is in its warm phase, these droughts tend to be more frequent or prolonged (NOAA 2005). As a result, the Great Lakes experience

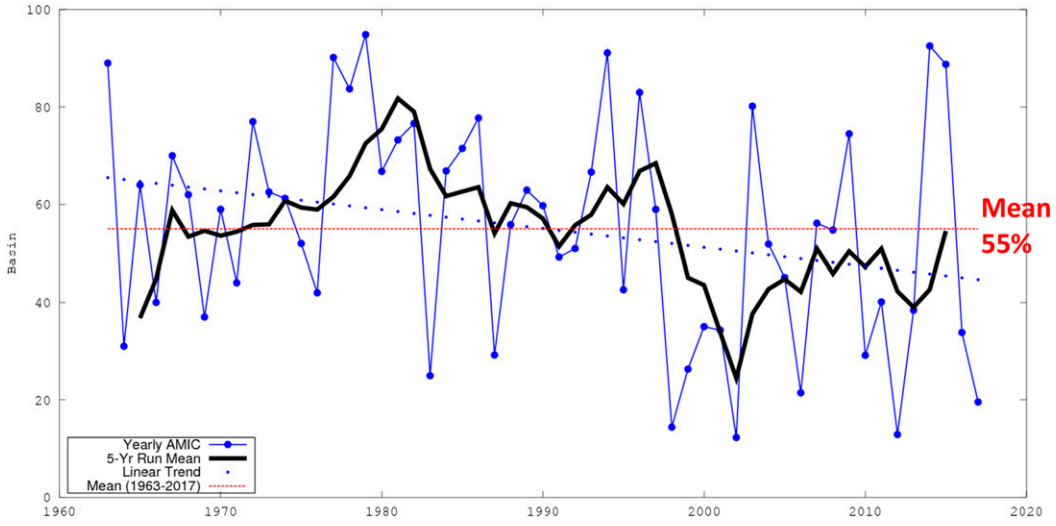

FIG. 3. Time series of AMIC during 1963–2017. The thick black line is the 5-yr running mean, indicating the decadal signal. The thin dashed red line is the climatological mean of 55%, and the blue dotted line indicates the long-term trend.

warmer-than-normal SAT and/or LST during the warm phase of AMO. The cold phase produces a cooling SAT and/or SST in the North Atlantic, as well as in the Great Lakes.

The correlation of ice cover with PDO is only 0.15, indicating that the linear correlation is poor (Figs. 5 and 6d and Table 1) with a comparable magnitude, but an opposite sign, to Niño-3.4 (−0.13). The quadratic PDO

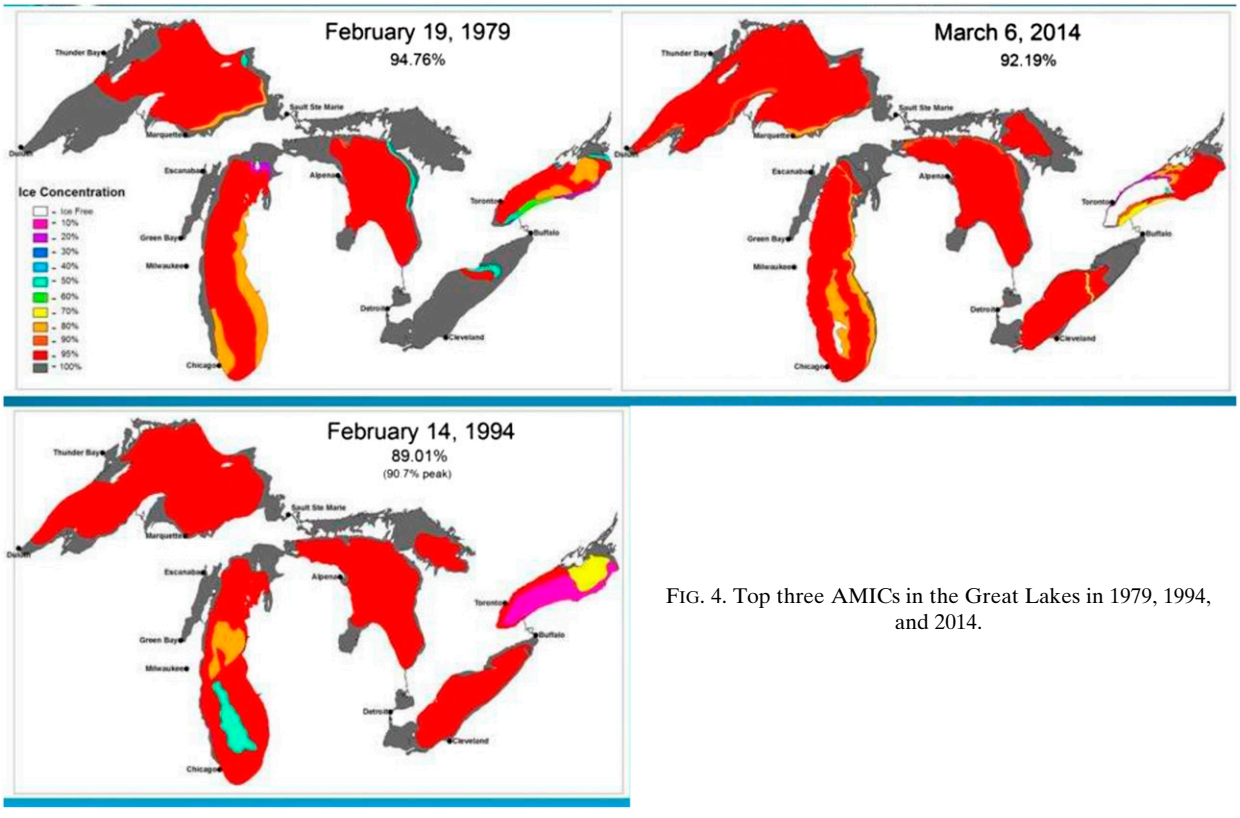

FIG. 4. Top three AMICs in the Great Lakes in 1979, 1994, and 2014.

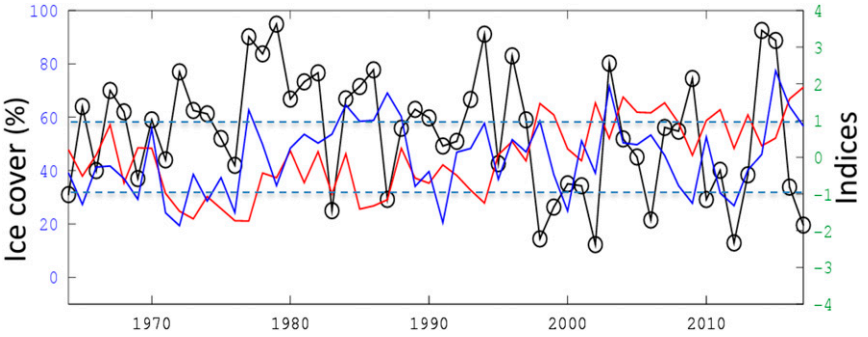

FIG. 5. The annual time series of AMIC (black), AMO index (red), and PDO index (blue). The linear correlation coefficients calculated are r(AMIC, AMO) = −0.38 and r(AMIC, PDO) = 0.15 (see also Table 1). The dashed lines denotes the indices >1 and <−1.

has a smaller coefficient (0.11) with ice cover, but with a comparable magnitude to the linear PDO. Although there is no statistical significant linear correlation (−0.13) between Niño-3.4 and AMIC, its quadratic term becomes much higher (−0.42) and is over the 99% significance level. NAO has a low correlation (−0.1) with AMIC at only 54% significance level during 1963–2017; however, its quadratic term has a much lower correlation with AMIC, indicating a weak linear correlation.

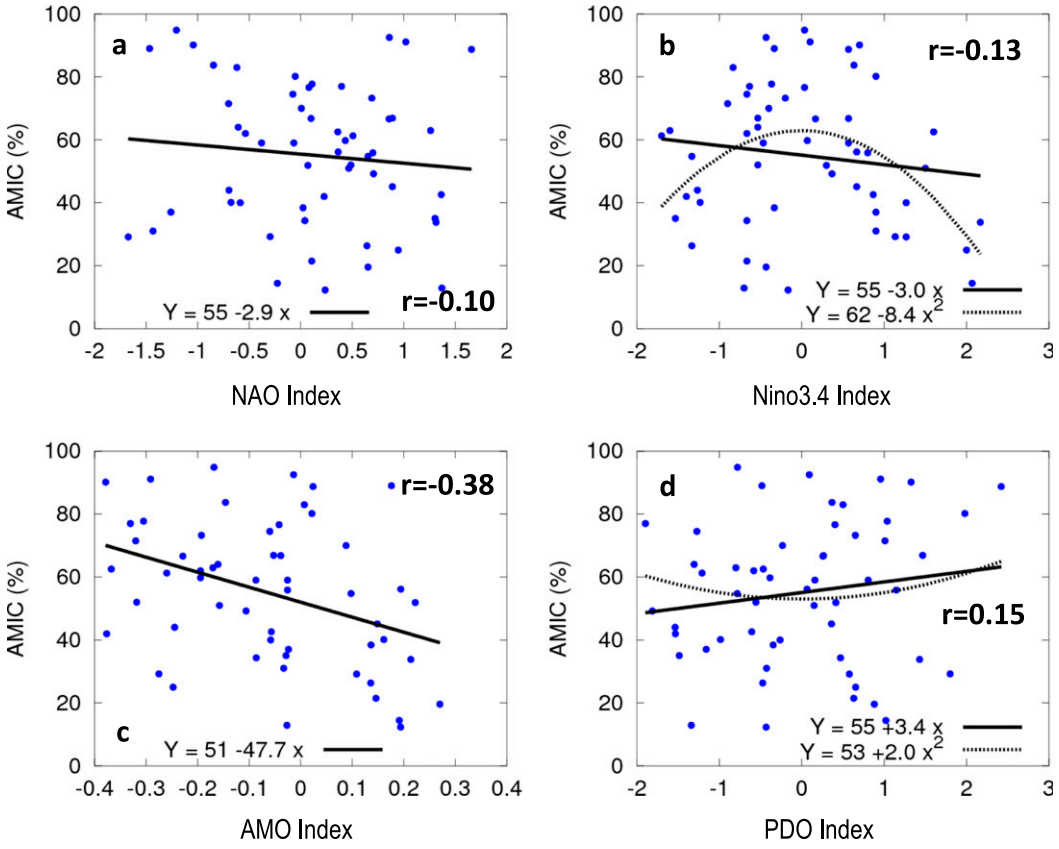

FIG. 6. Scatterplots of AMIC vs (a) NAO, (b) Niño-3.4, (c) AMO, and (d) PDO indices. The linear regression lines are given with solid black lines. The quadratic curves are also given for Niño-3.4 and PDO. The r indicates the linear correlation coefficients between the time series of AMIC and the individual indices for the period of 1963–2017. (see also Table 1).

TABLE 1. Correlations and p values of AMIC with teleconnection patterns. The coefficients in boldface are significant.

Index	r	p value	Significance (%)
Niño-3.4	−0.131	0.340	66
(Niño-3.4)^2	**−0.415**	0.002	**99.8**
NAO	−0.102	0.458	54.2
NAO^2	−0.004	0.979	1
AMO	**−0.377**	0.005	**99.5**
AMO^2	−0.096	0.484	51.6
PDO	0.151	0.271	62.9
PDO^2	0.109	0.429	57.1

However, the correlation between AMIC and AMO is −0.38 (Fig. 5 and Table 1), which is of the 99.5% significance level. Nevertheless, its quadratic index has a much lower correlation with AMIC, indicating that AMO acts as a linear forcing on ice cover. During the positive (warm) phase of AMO, there should be less ice cover in the Great Lakes; during the negative (cold) phase of AMO, there should be above-normal ice cover in the Great Lakes.

In summary, the above correlation analysis indicates that NAO and AMO have a linear correlation with AMIC, while ENSO and PDO have a nonlinear correlation with AMIC, although the nonlinear PDO has a slightly smaller coefficient with AMIC than its linear index, but with a comparable magnitude. Therefore, both linear and nonlinear impacts of ENSO and PDO should be included in any regression models, as discussed in section 5.

b. Scatter analysis

With seven years of data added to this study, the NAO has a smaller linear correlation ($r = -0.10$; Fig. 6a) with AMIC than that of Bai et al. (2012) ($r = -0.27$). The basic correlation remains unchanged. Niño-3.4 has a strong quadratic correlation with AMIC (Fig. 6b and Table 1). Similarly, the scatter analysis is applied to the AMO and PDO indices against AMIC (Figs. 6c,d), respectively. A linear regression can be obtained between the AMIC and AMO index (Fig. 6c) with a linear correlation of −0.38 at the 99.5% significance level. The scatterplot between the AMIC and PDO index shows a complicated picture with combined quadratic curve (dashed line; $r = 0.11$) and a weak linear correlation ($r = 0.15$) (Fig. 6d and Table 1). The quadratic curve between the AMIC and PDO is similar to Niño-3.4, but with opposite curvature and weak nonlinearity. It is noted that quadratic relation implies that high and low index values of Niño-3.4 would have a similar warming effect on lake ice. In other words, either a strong El Niño or a strong La Niña would lead to warming in the Great Lakes region, causing less ice cover; however, a stronger El Niño produces larger warming (i.e., less ice) than a strong La Niña. This asymmetric effect between the El Niño and La Niña events on ice cover was discussed by Bai et al. (2012).

In summary, the AMO has a negative correlation to AMIC, similar to the NAO; nevertheless, the correlation between ice cover and the AMO index ($r = -0.38$) is of 99.5% significance, while that with the NAO ($r = -0.1$) is not statistically significant, indicating that the AMO's impact should be important on decadal time scales. The PDO has a weak linear correlation with AMIC ($r = 0.15$) and a comparable quadratic correlation ($r = 0.11$) with AMIC. The PDO also has a positive correlation ($r = 0.11$), differing from the negative correlation between Niño-3.4 and AMIC ($r = -0.13$). Therefore, the interaction or competing process between the Niño-3.4 and PDO on Great Lakes ice cover on the crossing interannual and decadal time scales should be important for a regression model. A similar situation applies to the NAO and AMO. Furthermore, similar to the interaction or competing impact between the NAO and Niño-3.4 on interannual time scales, the interaction between the AMO and PDO on decadal time scales should be taken into account.

c. Correlation and composites of AMO and PDO

The impacts of teleconnection patterns in the Northern Hemisphere are well known (Fig. 7). NAO impact centers are in the Icelandic low and Azores high (Fig. 7a), while ENSO indicates the Pacific–North American (PNA) pattern (Fig. 7b), both of which were extensively investigated by Bai et al. (2012). The AMO pattern mimics the NAO pattern with influence spreading on larger areas including the Great Lakes, Far East, and the northern Pacific Ocean (Fig. 7c). The PDO mimics ENSO with major impacts on the northern Pacific Ocean and the Arctic (Fig. 7d).

A common feature is that the Great Lakes are not located in any action centers of these patterns, although the Atlantic low center of the AMO has a closer coverage over the Great Lakes. The low correlations between ice cover and teleconnection indices are reflected by the fact that the Great Lakes are located at the edge of the action centers for these four patterns. This indicates that the impact of any individual teleconnection patterns on Great Lakes regional climate and ice cover is not deterministic, except for an extreme event caused by one or more patterns, such as the 1998/99 and 2016/17 El Niño events.

Bai et al. (2012) first proposed the concept of competing (or interacting, or interfering) impact/forcing between ENSO and NAO on lake ice, because neither alone has high (significant) correlation with lake ice

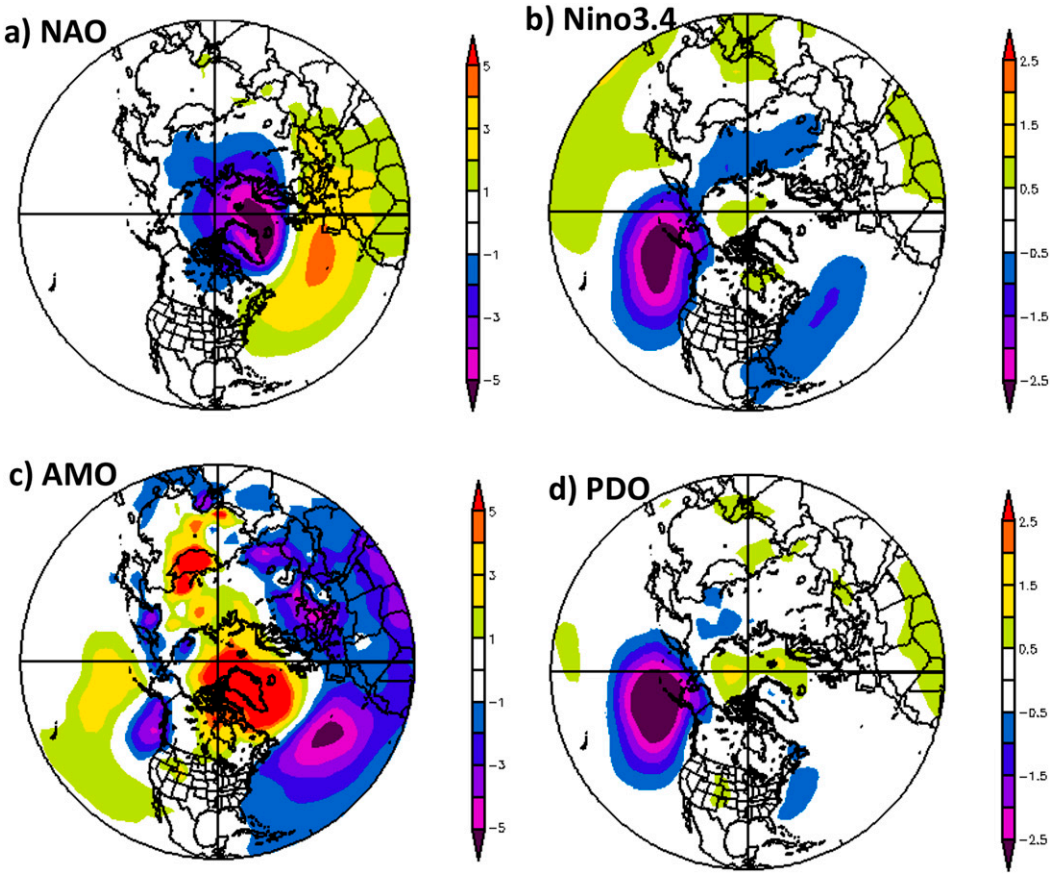

FIG. 7. Spatial regression map between the December–March (DJFM)-averaged SLP and indices of (a) NAO, (b) Niño-3.4, (c) AMO, and (d) PDO during 1949–2016. The color bars are in dynamic height (hPa).

because the Great Lakes are not located in any action center of both patterns, but rather at the edge of the action centers. This is reflected by the fact that AMIC has low linear correlation with ENSO, NAO, and PDO (not at 95% significance level), except for $r = 0.38$ with AMO at the 99.5% significance level as shown in Table 1. The four patterns actually coplay or coexist in the Great Lakes region. They often amplify the warming/cooling effects if they are in the same warming/cooling phase. However, when they are out of phase, such as warming versus cooling phase in one or more patterns, their joint effect can be partially canceled out. Therefore, the warming/cooling effect significantly weakens; this is the so-called interference. When one pattern stands out over the others, having much stronger impact on the region, this is the competing effect. This interaction, competing, or interference process is over the spatial distribution and time scales of these four patterns. Therefore, this in-phase or out-of-phase process on three time scales should be taken into account: interannual (ENSO vs NAO), decadal (AMO vs PDO), and crossing interannual and decadal (ENSO vs PDO and NAO vs AMO).

Figure 8 shows the spatial linear correlation map in North America between SAT and the four indices. There is positive correlation between the NAO and SAT over the Great Lakes region, indicating that the positive (negative) NAO leads to anomalous high (low) SAT (Fig. 8a). Similarly, over the Great Lakes region, ENSO in general has a positive correlation with local SAT, that is, El Niño (La Niña) leads to anomalous high (low) SAT (Fig. 8b). AMO has a strong positive correlation with SAT in Lakes Superior and Michigan and has a weak positive correlation with SAT in Lakes Huron and Ontario and has no correlation with SAT in Lake Erie (Fig. 8c). Interestingly, PDO has a weak positive correlation with SAT in Lake Superior, while a negative correlation with SAT in Lakes Erie and Ontario (Fig. 8d). PDO has negligible correlation with Lakes Michigan and Huron.

Lake Ontario is only half affected by PDO. The possible reasons are as follows: 1) Since Lake Ontario is located

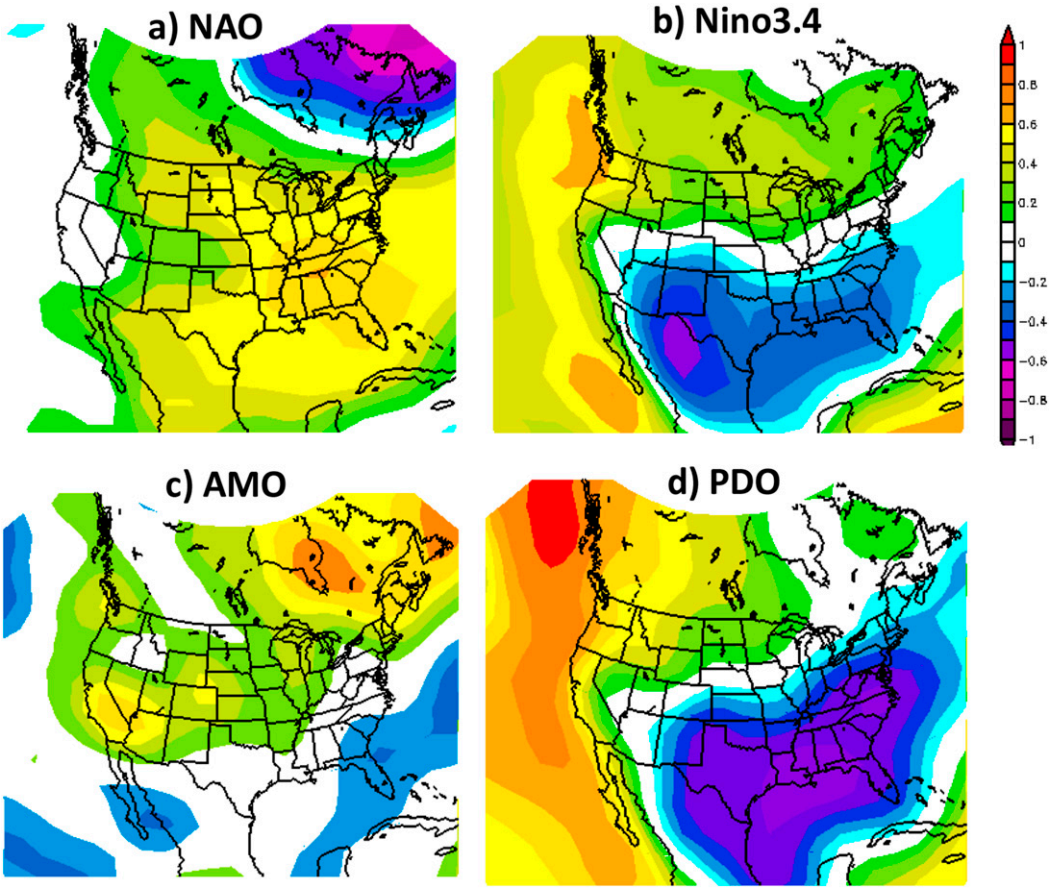

FIG. 8. Spatial linear correlation map between the SAT and DJFM indices of (a) NAO, (b) Niño-3.4, (c) AMO, and (d) PDO during 1949–2016.

near the negative center of PDO, SAT in the eastern Ontario is affected by the negative center. Note that although Lake Ontario is located at the edge of the two action centers (Fig. 8d), the negative center is much closer to the Great Lakes than the positive center that is located offshore of British Columbia, Canada; and 2) PDO has a weak linear relationship with AMIC (which is reversely correlated with SAT; see Table 1). This is similar to the nonlinearity of ENSO: the SAT pattern derived from ENSO has a zero line crossing the midbasin, that is, across Lake Ontario based on the EOF analysis (see Fig. 10b of Wang et al. 2012a). In addition, Lake Ontario is a deep-water lake in comparison, and has the lowest ice cover and largest standard deviation (i.e., variability, see Fig. 3 of Wang et al. 2012a). Because of the nonlinear effects of ENSO and PDO, and the large variability, Lake Ontario ice cover is the most difficult to predict.

To further reveal that Great Lakes LST is also impacted by the AMO and PDO, positive AMO (AMO+) and negative AMO (AMO−) years were selected for the period 1995–2017, during which satellite-measured LST data are available (AMO+ for 1998–2017, AMO− for 1995–97, PDO+ for 1995–98 and 2014–16, and PDO− for 2008–13). Figure 9 shows the winter SAT (Fig. 9a) and winter LST (Fig. 9b) difference between the AMO+ and AMO− years. AMO is positively correlated with both SAT and LST. During the positive AMO, there is a positive LST anomaly over four Great Lakes, except for Lake Erie and along the coast with ice cover, and vice versa during the negative AMO years. The LST difference along the coast and Lake Erie is near zero because 1) as shown in Fig. 8c, AMO has near-zero correlation with SAT in Lake Erie, and 2) ice-covered LST is near freezing temperature in both phases of AMO.

Figure 10 shows the cold SAT anomaly during the positive phase of PDO (PDO+; Fig. 10a) and warm SAT anomaly during the negative phase PDO (PDO−; Fig. 10b). As a result, the LST difference (Fig. 10c) between the positive and negative phase of PDO shows cold anomalies over most of the Great Lakes, except for Lake Erie and along the coast with

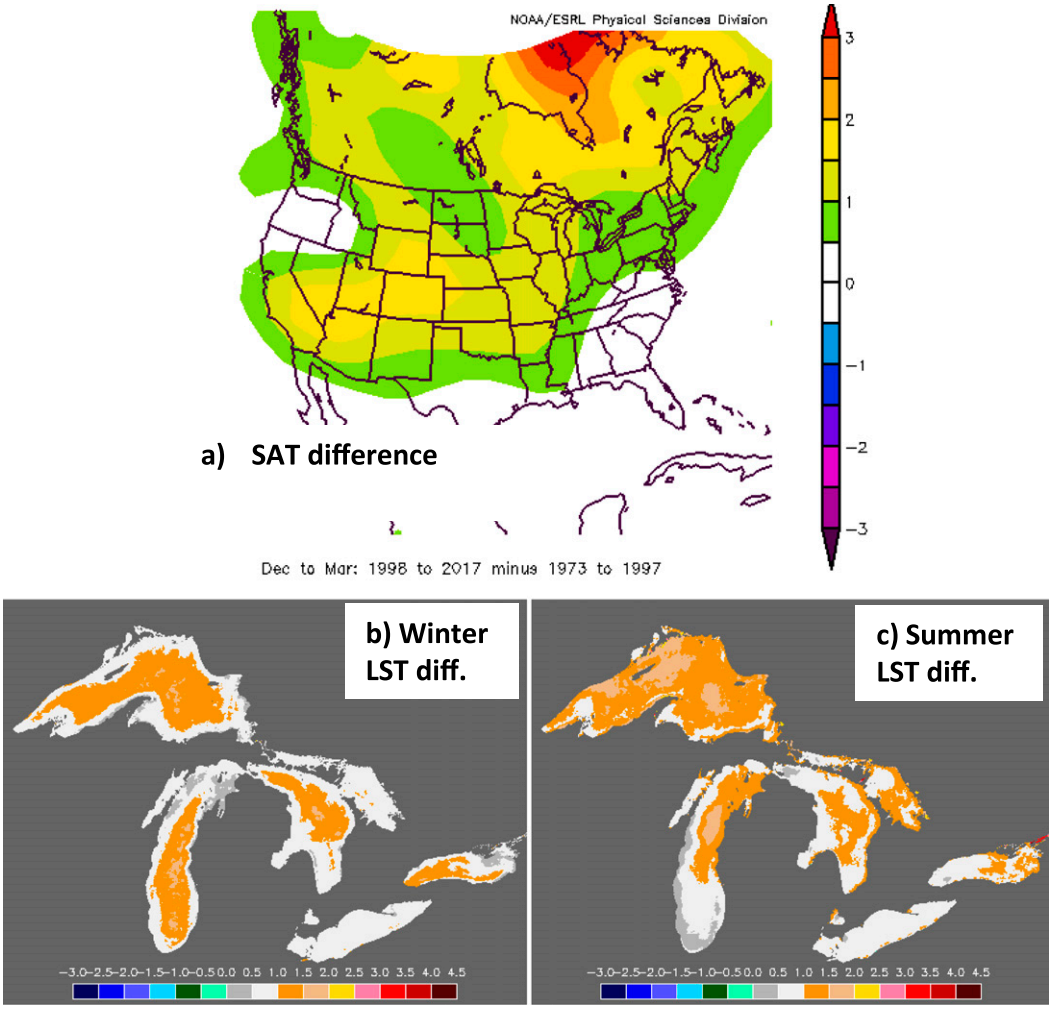

FIG. 9. Spatial difference (or anomaly) map between AMO+ years (1998–2017) and AMO− years (1973–97) for (a) SAT and (b) winter and (c) summer LST difference between the AMO+ and AMO− (°C).

ice cover nearly each year. Positive PDO leads to anomalous cold LST in most of the lakes, except for Lake Erie and along the coast with ice cover. During the negative phase of PDO, most of the Great Lakes experience a warm anomaly, except in Lake Superior: the western part experiences a cold anomaly, and the eastern part has zero anomaly (Fig. 10b).

The summer LST difference between the AMO+ and AMO− shows a warm anomaly (Fig. 9c) over the Great Lakes, except for Lake Erie, consistent with the winter warm anomaly (Fig. 9b). By contrast, the summer LST difference (Fig. 10d) between the PDO+ and PDO− shows a cold anomaly over the Great Lakes, except for Lake Erie, consistent with the winter cold anomaly (Fig. 10c). Therefore, Lake Erie LST in general is not as sensitive as other lakes with deeper water (i.e., larger heat content) in response to the decadal teleconnection forcing (see Figs. 9 and 10) because it is a shallow lake (mean depth of 19 m) in comparison to the other lakes (mean depth of Superior is 148 m, Michigan is 84 m, Huron is 59 m, and Ontario is 85 m; see Fig. 1). Thus, Lake Erie is generally ice-covered nearly every year, except for extremely warm winters such as 1983, 1991, 1998, 2002, 2006, 2012, and 2017; they were either strong El Niño, strong NAO+, or combined strong El Niño and NAO+ events (Bai et al. 2015).

d. Composite analysis of Great Lakes ice cover

Since lake ice cover has an inverse (i.e., negative) correlation with SAT ($r = \sim -0.8$; Bai et al. 2011, 2012) and LST ($r = -0.44$), it is expected that during the AMO+ (AMO−) and during the PDO− (PDO+) phase, there is anomalously less (more) ice cover in the Great Lakes. AMIC was selected in the following

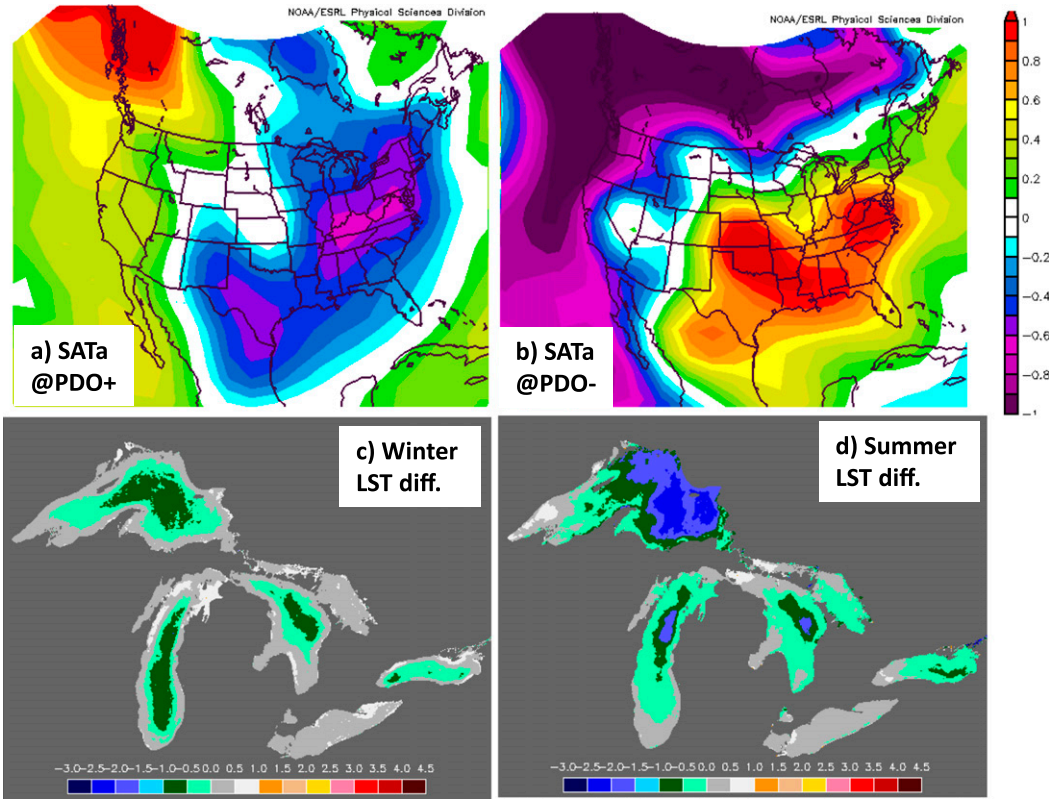

FIG. 10. Spatial composite DJFM SAT anomaly map referred to the climatology/mean of 1981–2010 for (a) PDO+ years and (b) PDO− years and (c) winter and (d) summer LST difference between PDO+ and PDO− (°C).

winters according to the AMO and PDO indices (see Fig. 5). The positive/warm phase of AMO has 14 winters: 1967, 1998, 1999, 2002, 2004, 2005, 2006, 2007, 2008, 2010, 2011, 2013, 2016, and 2017; and the negative/cold phase of AMO has 10 winters: 1972, 1973, 1974, 1975, 1976, 1983, 1985, 1986, 1987, and 1993. Since $n_1 = 14$ and $n_2 = 10$ [see Eq. (1)], the degrees of freedom are $14 + 10 - 2 = 22$. The positive (cold anomaly in the Great Lakes) phase of PDO has 12 winters: 1970, 1977, 1984, 1985, 1986, 1987, 1988, 1994, 1998, 2003, 2015, and 2016; and the negative (warm anomaly in the Great Lakes) phase of PDO has 10 winters: 1964, 1971, 1972, 1974, 1976, 1991, 2000, 2009, 2011, and 2012. Since $n_1 = 12$ and $n_2 = 10$ [see Eq. (1)], the degrees of freedom are $12 + 10 - 2 = 20$.

Figure 11 shows the composite mean ice cover of AMO+ (Fig. 11a) and AMO− (Fig. 11b) during the period 1963–2017. The ice cover difference (Fig. 11c) between the AMO+ and AMO− indicates less ice cover over the entire Great Lakes with the largest ice deficit being in Lake Superior. The Student's t test [Fig. 11d; see Eq. (1)] indicates that Lake Superior is the major region where AMO influence is noticed. Northern Lake Michigan and Lake Huron are very sensitive to AMO. These results are consistent with SAT and LST difference (Fig. 9).

Similar to AMO, Fig. 12 shows the composite mean ice cover of PDO+ (Fig. 12a) and PDO− (Fig. 12b) during the period 1963–2017. The ice cover difference (Fig. 12c) between the PDO+ and PDO− indicates more ice cover over the entire Great Lakes with the largest anomalous ice cover being in Lakes Michigan and Huron, eastern Superior, and eastern Ontario. The Student's t test (Fig. 12d) indicates that Lakes Michigan and Huron and eastern Lake Ontario are the major regions impacted by PDO. The PDO has no significant influence on ice cover in Lake Superior and Erie over the 95% significance level.

5. Development of multivariable regression models

Based on the investigation above, multivariable regression models can be constructed following Bai et al. (2012). The following model is the same as Bai et al. (2012) except that the data are now extended through 2017, and it only includes NAO, Niño-3.4, and their interaction (i.e., the competing term):

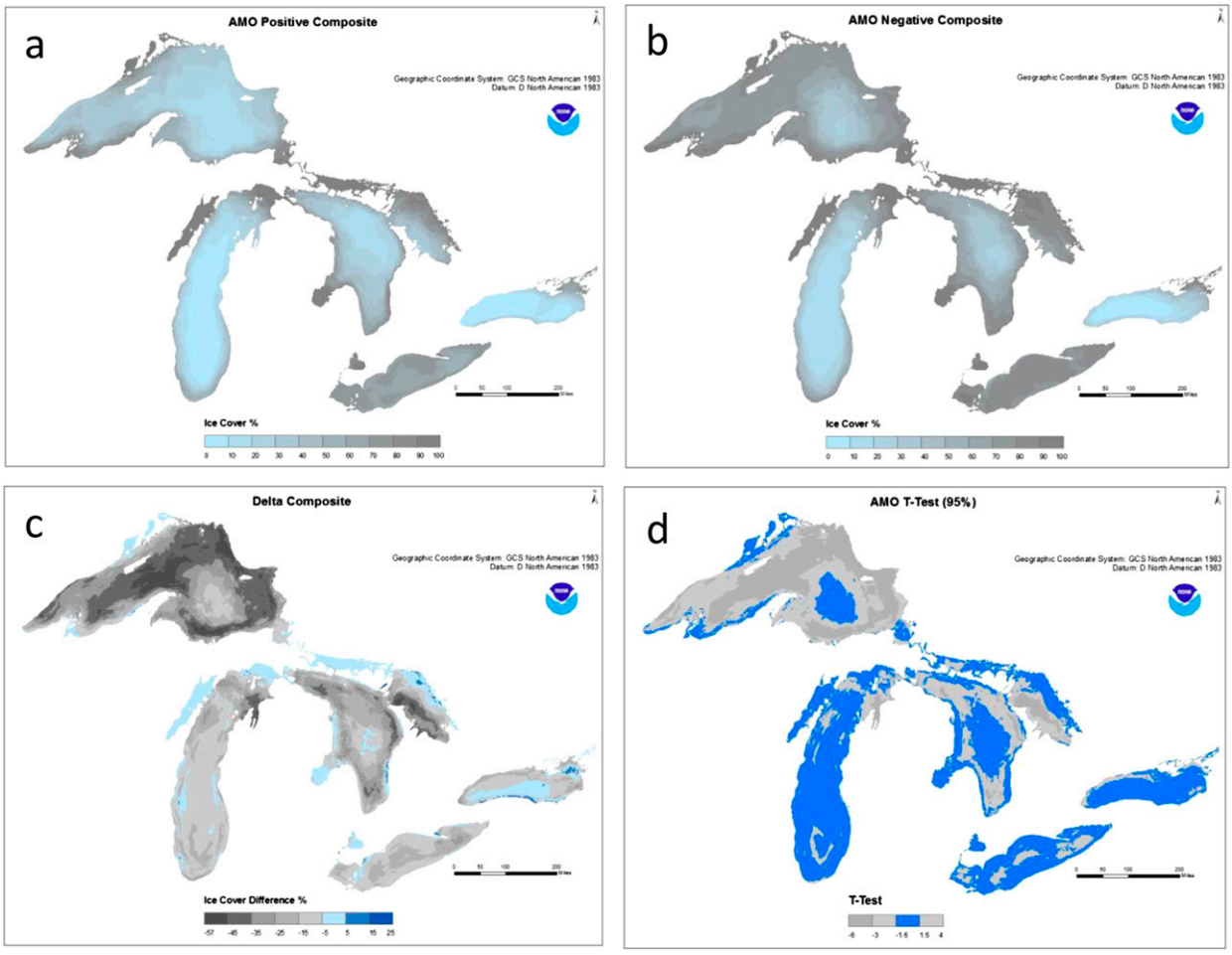

FIG. 11. Spatial composite AMIC during (a) AMO+ years, (b) AMO− years, (c) difference between AMO+ and AMO− years, and (d) Student's t test areas for over the 95% significance level.

$$Y = 0.46 - 0.02\text{Niño-3.4} - 0.5(\text{Niño-3.4})^2 - 0.33\text{NAO} + 0.29\text{NAO}(\text{Niño-3.4})^2, \quad (3)$$

where Y is normalized AMIC. The correlation between the model hindcast time series and the observed AMIC is $r = 0.48$ ($r^2 = 0.23$; see Fig. 13a).

As discussed above, the interaction or competing mechanisms of the teleconnection patterns on ice cover should be important. These competing mechanisms include 1) the NAO and Niño-3.4 on interannual time scales, as discussed in Bai et al. (2012); 2) the NAO and AMO and the Niño-3.4 and PDO on crossing interannual and decadal time scales; and 3) the AMO and PDO on decadal time scales. Thus, the following comprehensive, full regression model is constructed:

$$\begin{aligned} Y = {} & 0.32 - 0.18\text{Niño3.4} - 0.44(\text{Niño3.4})^2 - 0.44\text{NAO} + 0.32\text{NAO} \times (\text{Niño3.4})^2 \\ & - 0.58\text{AMO} + 0.28\text{PDO} + 0.18\text{PDO}^2 \\ & - 0.16\text{AMO} \times \text{NAO} - 0.08\text{PDO}^2 \times (\text{Niño3.4})^2 \\ & + 0.18\text{AMO} \times \text{PDO}^2. \end{aligned} \quad (4)$$

The correlation further increases from $r = 0.48$ ($r^2 = 0.23$) to 0.69 ($r^2 = 0.48$) in Eq. (3). Therefore, including the AMO and PDO and their interactions significantly improves the prediction skill (Fig. 13b) from the

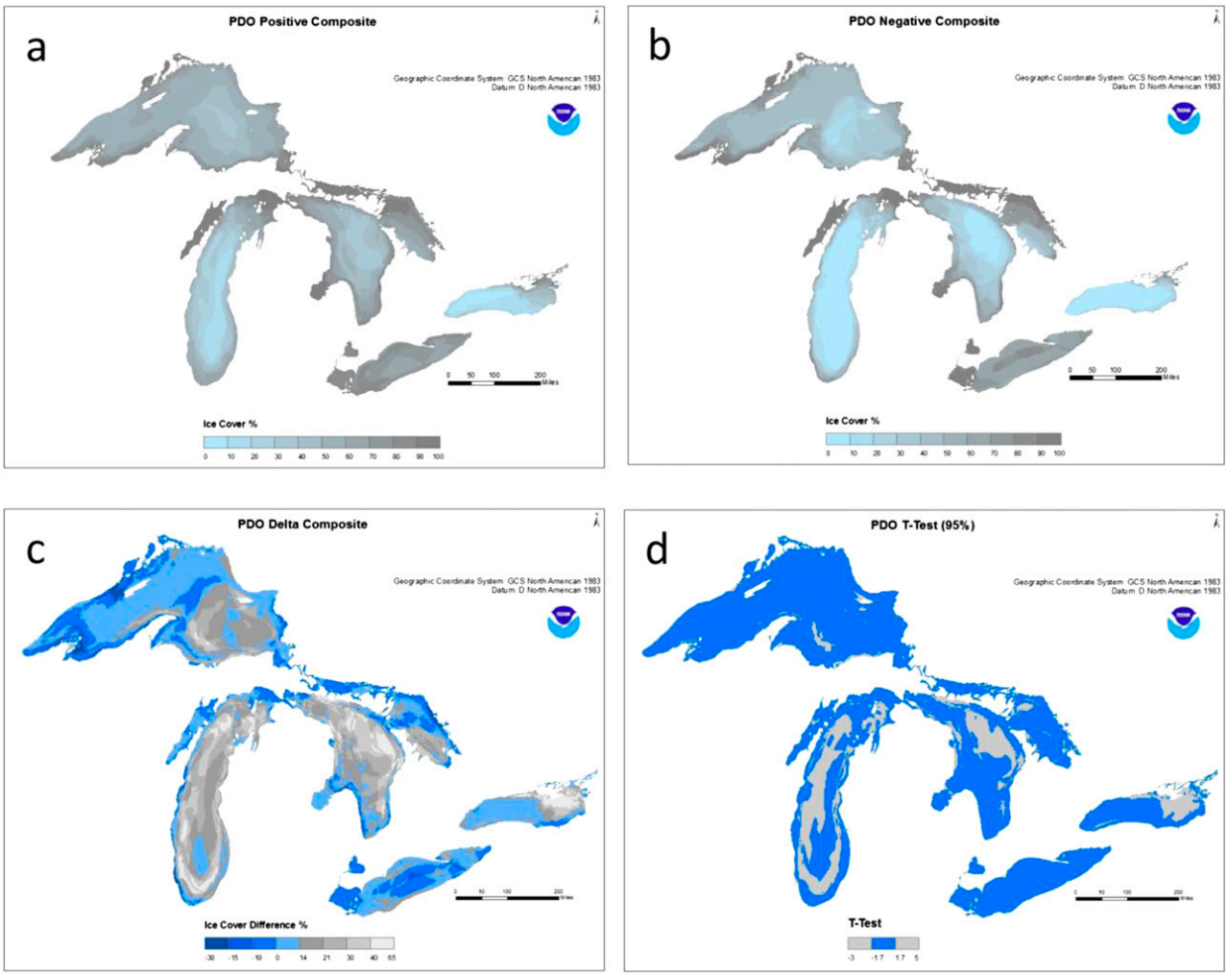

FIG. 12. Spatial composite AMIC during (a) PDO+ years, (b) PDO− years, (c) difference between PDO+ and PDO− years, and (d) the 95% significance level areas using the Student's *t* test.

original model that only includes the NAO and Niño-3.4 (Fig. 13a).

The statistics of the regression models versus measurements is listed in Table 2. The dynamical mechanisms for Eq. (4) (i.e., the full model) are as follows: The first row is the same as Bai et al. (2012) and only includes the NAO and Niño-3.4 and their competing effects on ice on interannual time scales. The second row includes the individual effect of linear AMO, PDO, and quadratic PDO on lake ice on decadal time scales. The third row represents the dynamical interactions or competing effects between the AMO and NAO and between nonlinear (quadratic) PDO and Niño-3.4 (Wu et al. 2005) on the crossing decadal and interannual time scales. The fourth row includes the competing effect between AMO and quadratic PDO on ice cover on decadal time scales.

Figure 13b shows the comparison between the full model and the observed AMIC, with the AMO and PDO included. Several important extremely high and low ice years were captured, compared with the original model that significantly underestimates the extreme events, such as in 1977–79, 1986, 1994, and 2003. Therefore, it is important to include the AMO and PDO patterns on decadal time scales, their interactions or competing impacts on the decadal time scales, and the competing impacts with the NAO and Niño-3.4 on interannual time scales in predicting Great Lakes ice cover.

As discussed above and in previous studies, LST has a close negative relationship with lake ice cover ($r = -0.44$), which needs to be considered. For the purpose of seasonal projection, November LST was chosen to predict lake ice cover in the coming winter. The reasons are 1) November is the month during which the Great Lakes are experiencing cooling and thus deep convection, but it is before the surface–bottom

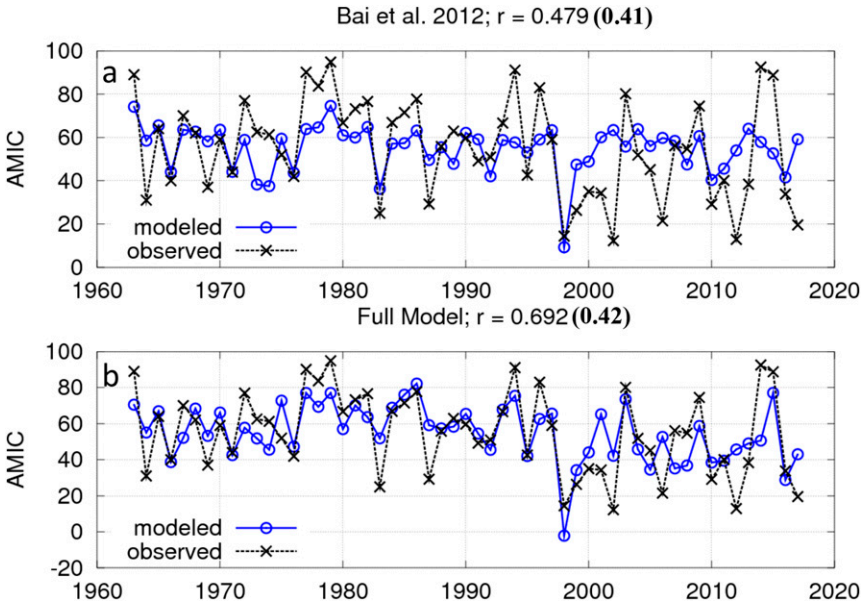

FIG. 13. (a) The hindcast using ENSO and NAO only (Bai et al. 2012) (in blue) and observed AMIC (black), and (b) as in (a), but with all the effects from the four patterns: NAO, AMO, Niño-3.4, and PDO, and their combined competing mechanisms. The corresponding linear correlation between the model results and the observed AMIC is given at the top of (a) and (b). The 95% significance criterion (coefficient, i.e., level) based on Monte Carlo simulation is provided in the parentheses.

overturning that often occurs in December when lake surface temperature drops to 4°C. Therefore, November LST has larger variability than does December, and is an ideal preconditioning temperature for timing the formation of lake ice; and 2) in early–mid-December, we would like to make projections of maximum ice cover into winter (usually occurs in late January–early March). At the time, we can collect November temperature for all the lakes.

There are two types of LST data in the Great Lakes: 1) satellite measurement as introduced in section 2c starting from 1995 to the present, and 2) buoy in situ measured LST starting from 1982 to 2016. The linear correlation between the two time series is 0.79, and that between the buoy LST and AMIC is −0.44. We constructed regression models using both data and the results are consistent to each other. Therefore, we chose the buoy data because they cover a longer period.

When LST only was used to hindcast the ice cover, the correlation between the model result and the ice cover is $r = 0.46$ (not shown), which is higher than the correlation (0.48; Fig. 13a) using the NAO and Niño-3.4 indices only (Bai et al. 2012). When combining LST, NAO, and Niño-3.4, the correlation between the hindcast time series and measurement increases to 0.58 (not shown). To compare the performance of the full models with and without LST during the shortened period 1982–2016, the full regression model including all four teleconnection patterns [Eq. (4)] without November LST is constructed as follows:

TABLE 2. Statistics of the multiple variable regression models using data from 1963 to 2017 and from 1982 to 2017. The coefficients in boldface are significant. [Correlation is Pearson's correlation coefficient r; p value is the probability this correlation would happen by random chance; adj r^2 is r^2 adjusted (this is important for multiple variable regression); within 20% is the percentage of years that model predicted within 20% of observed (less than 20% absolute error); and within 10% is same as within 20%, but for 10%.]

	Data used	RMSE	Correlation	p value	r^2	Adj r^2	Within 20%	Within 10%
ENSO and NAO	1963–2017	20.49	**0.48**	2.3×10^{-4}	0.23	0.17	65%	38%
Full model	1963–2017	17.95	**0.69**	5.4×10^{-9}	0.48	0.36	78%	47%
Full model	1982–2017	19.18	**0.71**	1.1×10^{-6}	0.50	0.31	75%	53%
Full model with LST	1982–2017	17.45	**0.78**	2.1×10^{-8}	0.61	0.43	83%	58%

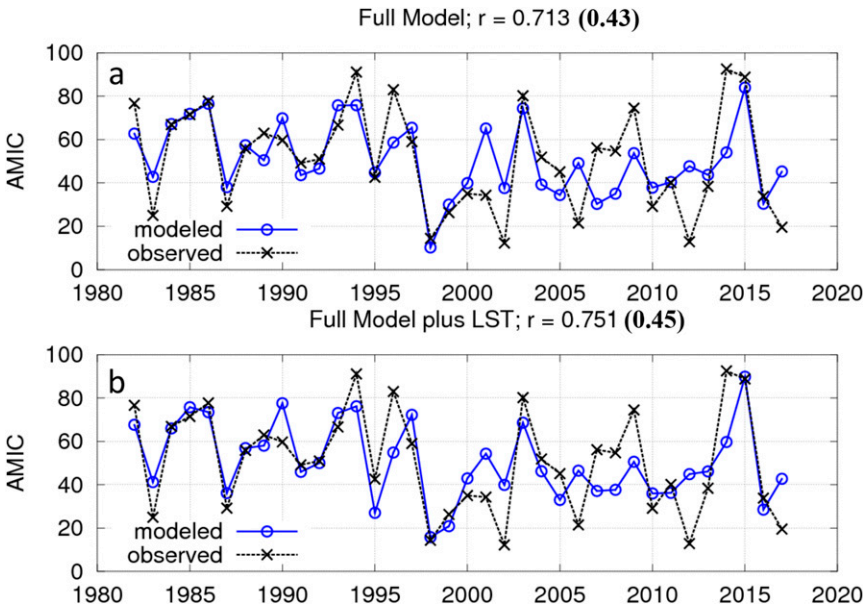

FIG. 14. (a) As in Fig. 13b, but with the period 1982–2016. (b) As in (a), but the full model with November LST.

$$\begin{aligned} Y = {} & 0.57 - 0.18\text{Niño3.4} - 0.42(\text{Niño3.4})^2 - 0.20\text{NAO} + 0.13\text{NAO} \times (\text{Niño3.4})^2 \\ & - 3.90\text{AMO} + 0.25\text{PDO} - 0.04\text{PDO}^2 \\ & - 0.58\text{AMO} \times \text{NAO} - 0.01\,\text{PDO}^2 \times (\text{Niño3.4})^2 \\ & + 2.35\text{AMO} \times \text{PDO}^2, \end{aligned} \tag{5}$$

and with November LST (in °C) was constructed as follows:

$$\begin{aligned} Y = {} & 0.30 - 0.19\text{Niño3.4} - 0.39(\text{Niño3.4})^2 - 0.05\text{NAO} + 0.04\text{NAO} \times (\text{Niño3.4})^2 \\ & - 0.67\text{AMO} + 0.27\text{PDO} - 0.12\text{PDO}^2 \\ & - 0.001\text{AMO} \times \text{NAO} + 0.01\text{PDO}^2 \times (\text{Niño3.4})^2 \\ & + 0.53\text{AMO} \times \text{PDO}^2 \\ & - 0.35\text{LST}, \end{aligned} \tag{6}$$

where LST is the normalized November LST with a mean of 8.11°C and standard deviation of 0.83°C. The correlation between the hindcast ice cover and measured ice cover during the period 1982–2016 without LST [with Eq. (5)] is $r = 0.71$ ($r^2 = 0.5$; see Fig. 14a). With LST included, the correlation significantly increases to 0.78 ($r^2 = 0.61$; Fig. 14b). The statistics of both models are also listed in Table 2. Therefore, November LST is a key parameter to hindcast lake ice cover because it provides a preconditioning of lake ice formation.

In summary, as Table 2 indicates, all four regression models are statistically significant. The hindcast skill of the full model [Eq. (4)] is significantly improved, capturing 48% of the total variance, compared to only 23% by using ENSO and NAO indices only [Eq. (3)] for the period 1963–2017. With November LST included to the full model [Eq. (6)] for the period 1982–2016, the hindcast skill is also significantly increased by capturing 61% of the total variance, compared to 50% in the full model without LST.

To further confirm that the regression models using the full time series better represent both climate dynamics and statistical properties, a jackknifing method was used to investigate the RMSEs of the regression models using only a subset of the data, as discussed in detail in the appendix.

6. Conclusions and discussion

On the basis of the above investigation, the following conclusions can be drawn.

1) It is found that the AMO has a negative linear correlation ($r = -0.38$) with AMIC at the 99.5% significance level, in a similar manner to, but larger than, the NAO ($r = -0.10$). The PDO has a weak linear correlation ($r = 0.15$) with AMIC, similar to, but with the opposite curvature of the Niño-3.4 ($r = -0.13$). However, both PDO and Niño-3.4 have nonlinear effects on Great Lakes ice cover.
2) During the positive (negative) AMO events, SAT over the Great Lakes and LST have positive (negative) anomalies. As a result, there is less (more) lake ice cover in the Great Lakes during the positive (negative) AMO phase. The Student's t test shows that the primary impact region includes Lake Superior, Lake Huron, and northern Lake Michigan. During the positive (negative) PDO events, SAT over the Great Lakes and LST have negative (positive) anomalies. Accordingly, there is more (less) lake ice cover in the Great Lakes during the positive (negative) PDO phase. The Student's t test shows that the major impact region includes Lake Huron, Lake Michigan, and eastern Lake Ontario.
3) Comprehensive regression hindcast models were developed using all four teleconnection patterns: NAO and Niño-3.4 on interannual time scales, and AMO and PDO on decadal time scales. The full model constructed here can capture 48% of the total variance of ice cover, compared to only 23% of Bai et al. (2012). The correlation between the hindcast model results and observations is 0.69. This model includes not only the interactions/competing effects within interannual time scales (NAO and Niño-3.4) and within decadal time scales (AMO and PDO), but also includes the competing effects across interannual and decadal time scales such as within Niño-3.4 and PDO, and within NAO and AMO.
4) When November LST was added to the equation, the hindcast skill is significantly improved from $r = 0.71$ ($r^2 = 0.50$) to 0.78 ($r^2 = 0.61$); that is, the total variance explained by the model increases from 50% to 61%. This indicates that the late-autumn preconditioning of lake surface temperature and heat content has significant contribution to lake ice formation in the coming winter.

In the appendix, it is shown that since the climate system is a nonstationary stochastic process and has multidecadal time periods, the jackknifing method may not be suitable to construct the regression models using only a subset of the 55-yr data. However, this method may be suitable for the stationary stochastic processes such as ocean surface waves.

It is important to note that there is a decreasing trend in the AMIC during the period 1963–2017 (see Fig. 3). The portion of the decrease that can be attributed to anthropogenic climate change (ACC) is unknown. For purposes of the multivariable regression analysis, the contribution of ACC to this observed change in ice cover is assumed to be negligible, compared to the AMO. While the AMO is defined by the residual SST anomaly after detrending North Atlantic water temperatures over a much longer period starting around 1880, which might also detrend portion of the long-term upward trend of ACC. When considering only the 1963–2017 period, the AMO has a distinct upward trend. Since the other indices do not have this distinct positive trend over the period of interest, the multiple regression models identify the positive trend in AMO as a main contributor to the downward trend in AMIC, even though ACC may also be a contributor, it is not included in the regression models of this study.

A challenge for the quantitative description of the relationship between AMIC and individual teleconnection patterns is that the correlation is not statistically significant such as with the PDO, Niño-3.4, and NAO. This had long been a barrier in the past several decades for scientists to achieve a hindcast model until the study of Bai et al. (2012). A combination approach using both Niño-3.4 and NAO patterns was proven to reasonably reproduce AMIC, although not perfectly (Bai et al. 2012). Based on the same idea, this study further includes the AMO and PDO and their interactions on decadal time scales and the interactions with interannual time scales (Niño-3.4 and NAO), as well as LST. The hindcast model was further improved. This hindcast model will be used to project seasonal AMIC in the next few years, whose predictability skills will be evaluated for a further improvement.

TABLE A1. RMSEs are estimated using the jackknifing method. The correlation coefficients and p value are derived. First half refers to the model that uses the first half of the data for training and predicts the second half (second half refers to the opposite; the second half is used as the training set and the first half is the prediction interval). The coefficients in boldface are significant.

	First half			Second half		
Model	RMSE	r	p value	RMSE	r	p value
Bai et al. (2012)	28.05	**0.26**	0.16	21.69	**0.46**	0.01
Full	31.59	0.18	0.34	30.00	0.16	0.45
Full short	36.55	0.17	0.51	31.34	0.12	0.66
Full + LST	36.81	0.16	0.51	84.81	0.30	0.23

Acknowledgments. NCEP reanalysis data were provided by the NOAA/OAR/ESRL Physical Sciences Division (PSD), Boulder, Colorado, from their website at http://www.cdc.noaa.gov/. Support from U.S. EPA's Great Lakes Restoration Initiative (GLRI) to climate change and modeling studies is appreciated. We appreciate Ms. Nicole Rice for her editorial assistance. We

TABLE A2. RMSEs and correlations are computed from each regression model using the jackknifing method: randomly training 70% of the data to hindcast the remaining 30% of the data. The p values for each correlation are provided.

Model	Ensemble_RMSE		Ensemble_r		p value	95% criterion min for r(prediction, obs)
	Mean	Std dev	Mean	Std dev		
Bai et al. (2012)	21.81	3.23	0.35	0.21	0.155	0.46
Full	22.50	3.65	0.44	0.19	0.084	0.48
Full short	27.00	7.78	0.34	0.27	0.301	0.60
Full + LST	27.78	9.43	0.39	0.26	0.252	0.60

also appreciate programming support from Songzhi Liu of University of Michigan Cooperative Institute for Great Lakes Research (CIGLR) for lake surface temperature. The authors deeply appreciated the constructive, two-round reviews by three anonymous, responsible experts, which indeed helped significantly improve the quality of the work. This is GLERL Contribution No. 1885. Funding was awarded to Cooperative Institute for Great Lakes Research (CIGLR) through the NOAA Cooperative Agreement with the University of Michigan (NA17OAR4320152). This is CIGLR Contribution No. 1127.

APPENDIX

Jackknifing Analyses of Regression Models

To further confirm that the regression models in Eqs. (3)–(6) are robust, the jackknifing method was suggested to be applied to the data to cross check the model's skills. Two experiments were conducted. First, a quick estimate of RMSE can be obtained by training the model (finding the model coefficients) on the first half of the data, then using this model to predict the second half of the data. The resulting RMSE would reflect the real predictive skill of the model. Conversely, we train the model on the second half of the data and use it to predict the first half. Table A1 shows the RMSEs that are derived from the jackknifing method.

It is clear that using one half of the data to hindcast the other half leads to an increase in RMSE, particularly when 1) more predictors, especially decadal predictors, are included (e.g., full model and full short + LST), and 2) the time series are short.

As we know, the climate system is a nonstationary stochastic process. A climate shift in lake ice in 1998 (Van Cleave et al. 2014) is evidence of nonstationarity, similar to other subsystems of the global climate (Milly et al. 2008; Razavi et al. 2015; among others). Based on Fig. 3, neither annual data nor the 5-yr running mean is stationary. The 55-yr data barely cover one cycle of AMO of a 50–70-yr period. Therefore, using the first half of the data with a different mean climate system (e.g., a negative AMO phase) to hindcast the second half (e.g., a positive AMO phase) contradicts the climate dynamics and nonstationarity. This is why RMSE significantly increases.

Furthermore, we randomly picked 70% of the data (to increase the training period length) to fit the model (find model coefficients), then computed RMSE using model predictions for the remaining 30% of the data. We repeated this 1000 times with different random subsamples (training/validation) of the data. The resulting estimates of RMSE would provide the ensemble mean and the RMSE values. This process would reflect the true predictive potential of each model if the climate system is not a nonstationary stochastic process. Each model was repeated to examine whether or not including more predictors increases the true hindcast skill. The correlation values between the observed and predicted time series were calculated. Table A2 shows both the RMSEs and correlation with p values.

It is shown that 1) including more predictors increases the true hindcast skills in terms of correlation and p value, while RMSE virtually remains the same, which is consistent with Table 2 using the full time series, and 2) the longer the time series, the lower the RMSE. The reason is because models derived from all the realizations (samples or data points) [Eqs. (3)–(6)] extract all dynamic processes (or cycles), which include as many as both positive and negative phases of the oscillations.

The limitation of the jackknifing method for the climate system is that the climate system is a nonstationary stochastic process, with climate shifts. A 30-yr period, as a conventional rule of thumb for a climatological mean, may not be representative of long-term climate and lake ice processes because of multidecadal oscillations, such as the AMO that has a 50–70-yr period. Nevertheless, the jackknifing method may be suitable for stationary stochastic processes such as ocean surface waves.

REFERENCES

Assel, R. A., and S. Rodionov, 1998: Atmospheric teleconnections for annual maximum ice cover on the Laurentian Great Lakes. *Int. J. Climatol.*, **18**, 425–442, https://doi.org/10.1002/(SICI)1097-0088(19980330)18:4<425::AID-JOC258>3.0.CO;2-Q.

——, K. Cronk, and D. C. Norton, 2003: Recent trends in Laurentian Great Lakes ice cover. *Climatic Change*, **57**, 185–204, https://doi.org/10.1023/A:1022140604052.

Bai, X., and J. Wang, 2012: Atmospheric teleconnection patterns associated with severe and mild ice cover on the Great Lakes, 1963–2011. *Water Qual. Res. J. Canada*, **47**, 421–435, https://doi.org/10.2166/wqrjc.2012.009.

——, ——, Q. Liu, D. Wang, and Y. Liu, 2011: Severe ice conditions in the Bohai Sea, China, and mild ice conditions in the Great Lakes during the 2009/10 winter : Links to El Niño and a strong negative Arctic Oscillation. *J. Appl. Meteor. Climatol.*, **50**, 1922–1935, https://doi.org/10.1175/2011JAMC2675.1.

——, ——, C. Sellinger, A. Clites, and R. A. Assel, 2012: Interannual variability of Great Lakes ice cover and its relationship to NAO and ENSO. *J. Geophys. Res.*, **177**, C03002, https://doi.org/10.1029/2010JC006932.

——, and Coauthors, 2015: A record-breaking low ice cover over the Great Lakes during winter 2011/2012: Combined effects of a strong positive NAO and La Niña. *Climate Dyn.*, **44**, 1187–1213, https://doi.org/10.1007/s00382-014-2225-2.

Clites, A. H., J. Wang, K. B. Campbell, A. D. Gronewold, R. A. Assel, X. Bai, and G. A. Leshkevich, 2014: Cold water and high ice cover on Great Lakes in spring 2014. *Eos, Trans. Amer. Geophys. Union*, **95**, 305–306, https://doi.org/10.1002/2014EO340001.

Ghanbari, R. N., H. R. Bravo, J. J. Magnuson, W. G. Hyzer, and B. J. Benson, 2009: Coherence between lake ice cover, local climate and teleconnections (Lake Mendota, Wisconsin). *J. Hydrol.*, **374**, 282–293, https://doi.org/10.1016/j.jhydrol.2009.06.024.

Livezey, R. E., and W. Y. Chen, 1983: Statistical field significance and its determination by Monte Carlo techniques. *Mon. Wea. Rev.*, **111**, 46–59, https://doi.org/10.1175/1520-0493(1983)111<0046:SFSAID>2.0.CO;2.

Magnuson, J. J., and Coauthors, 2000: Historical trends in lake and river ice cover in the Northern Hemisphere. *Science*, **289**, 1743–1746, https://doi.org/10.1126/science.289.5485.1743.

Mantua, N. J., S. R. Hare, Y. Zhang, J. M. Wallace, and R. C. Francis, 1997: A Pacific interdecadal climate oscillation with impacts on salmon production. *Bull. Amer. Meteor. Soc.*, **78**, 1069–1079, https://doi.org/10.1175/1520-0477(1997)078<1069:APICOW>2.0.CO;2.

Milly, P. C. D., J. Betancourt, M. Falkenmark, R. M. Hirsch, Z. W. Kundzewicz, D. P. Lettenmaier, and R. J. Stouffer, 2008: Stationarity is dead: Whither water management? *Science*, **319**, 573–574, https://doi.org/10.1126/science.1151915.

Mishra, V., K. A. Cherkauer, L. C. Bowling, and M. Huber, 2011: Lake ice phenology of small lakes: Impacts of climate variability in the Great Lakes region. *Global Planet. Change*, **76**, 166–185, https://doi.org/10.1016/j.gloplacha.2011.01.004.

NOAA, 2005: National Oceanic and Atmospheric Administration frequently asked questions about the Atlantic multidecadal oscillation (AMO). NOAA Physical Oceanography Division, https://web.archive.org/web/20051126030955/http://www.aoml.noaa.gov/phod/amo_faq.php.

Razavi, S., A. Elshorbagy, H. Wheater, and D. Sauchyn, 2015: Toward understanding nonstationarity in climate and hydrology through tree ring proxy records. *Water Resour. Res.*, **51**, 1813–1830, https://doi.org/10.1002/2014WR015696.

Schlesinger, M. E., and N. Ramankutty, 1994: An oscillation in the global climate system of period 65–70 years. *Nature*, **367**, 723–726, https://doi.org/10.1038/367723a0.

Ting, M., Y. Kushnir, R. Seager, and C. Li, 2009: Forced and internal twentieth-century SST trends in the North Atlantic. *J. Climate*, **22**, 1469–1481, https://doi.org/10.1175/2008JCLI2561.1.

Van Cleave, K., J. D. Lenters, J. Wang, and E. M. Verhamme, 2014: A regime shift in Lake Superior ice cover, evaporation, and water temperature following the warm El Niño winter of 1997–98. *Limnol. Oceanogr.*, **59**, 1889–1898, https://doi.org/10.4319/lo.2014.59.6.1889.

Wang, J., L. A. Mysak, and R. G. Ingram, 1994: Interannual variability of sea-ice cover in Hudson Bay, Baffin Bay and the Labrador Sea. *Atmos.–Ocean*, **32**, 421–447, https://doi.org/10.1080/07055900.1994.9649505.

——, X. Bai, G. Leshkevich, M. Colton, A. Clites, and B. Lofgren, 2010: Severe ice cover on Great Lakes during winter 2008–2009. *Eos, Trans. Amer. Geophys. Union*, **91**, 41–42, https://doi.org/10.1029/2010EO050001; Corrigendum, **93**, 136, https://doi.org/10.1029/2012EO130005.

——, ——, H. Hu, A. Clites, M. Colton, and B. Lofgren, 2012a: Temporal and spatial variability of Great Lakes ice cover, 1973–2010. *J. Climate*, **25**, 1318–1329, https://doi.org/10.1175/2011JCLI4066.1.

——, R. A. Assel, S. Walterscheid, A. H. Clites, and X. Bai, 2012b: Great Lakes ice climatology update: Winter 2006–2011 description of the digital ice cover dataset. NOAA Tech. Memo. GLERL-155, 37 pp., https://www.glerl.noaa.gov/pubs/tech_reports/glerl-155/tm-155.pdf.

——, J. Kessler, F. Hang, H. Hu, A. H. Clites, and P. Chu, 2017a: Great Lakes ice climatology update of winters 2012–2017: Seasonal cycle, interannual variability, decadal variability, and trend for the period 1973–2017. NOAA Tech. Memo. GLERL-170, 14 pp., https://www.glerl.noaa.gov/pubs/tech_reports/glerl-170/tm-170.pdf.

——, ——, ——, ——, ——, and ——, 2017b: Analysis of Great Lakes ice cover climatology: Winters 2012–2017. NOAA Tech. Memo. GLERL-171, 24 pp., https://www.glerl.noaa.gov/pubs/tech_reports/glerl-171/tm-171.pdf.

Weyhenmeyer, G. A., D. M. Livingstone, M. Meili, O. Jensen, B. J. Benson, and J. J. Magnuson, 2011: Large geographical differences in the sensitivity of ice-covered lakes and rivers in the Northern Hemisphere to temperature changes. *Global Change Biol.*, **17**, 268–275, https://doi.org/10.1111/j.1365-2486.2010.02249.x.

Wu, A., W. W. Hsieh, and A. Shabbar, 2005: The nonlinear patterns of North American winter temperature and precipitation associated with ENSO. *J. Climate*, **18**, 1736–1752, https://doi.org/10.1175/JCLI3372.1.

Zhang, R., and T. L. Delworth, 2006: Impact of Atlantic multidecadal oscillations on India/Sahel rainfall and Atlantic hurricanes. *Geophys. Res. Lett.*, **33**, L17712, https://doi.org/10.1029/2006GL026267.

Zhang, Y., J. M. Wallace, and D. S. Battisti, 1997: ENSO-like interdecadal variability: 1900–93. *J. Climate*, **10**, 1004–1020, https://doi.org/10.1175/1520-0442(1997)010<1004:ELIV>2.0.CO;2.